Ferromagnetic Resonance Spin Pumping and Electrical Spin Injection in Silicon-Based Metal-Oxide-Semiconductor Heterostructures

Y. Pu,[1,*] P. M. Odenthal,[2] R. Adur,[1] J. Beardsley,[1] A. G. Swartz,[2] D. V. Pelekhov,[1] M. E. Flatté,[3] R. K. Kawakami,[1,2] J. Pelz,[1] P. C. Hammel,[1] and E. Johnston-Halperin[1,†]

[1]*Department of Physics, The Ohio State University, Columbus, Ohio 43210, USA*

[2]*Department of Physics and Astronomy, University of California, Riverside, California 92521, USA*

[3]*Departent of Physics and Astronomy, University of Iowa, Iowa City, Iowa 52242, USA*

(Received 15 January 2015; published 10 December 2015)

We present the measurement of ferromagnetic resonance (FMR-)driven spin pumping and three-terminal electrical spin injection within the same silicon-based device. Both effects manifest in a dc spin accumulation voltage V_s that is suppressed as an applied field is rotated to the out-of-plane direction, i.e., the oblique Hanle geometry. Comparison of V_s between these two spin injection mechanisms reveals an anomalously strong suppression of FMR-driven spin pumping with increasing out-of-plane field H^z_{app}. We propose that the presence of the large ac component to the spin current generated by the spin pumping approach, expected to exceed the dc value by 2 orders of magnitude, is the origin of this discrepancy through its influence on the spin dynamics at the oxide-silicon interface. This convolution, wherein the dynamics of both the injector and the interface play a significant role in the spin accumulation, represents a new regime for spin injection that is not well described by existing models of either FMR-driven spin pumping or electrical spin injection.

DOI: 10.1103/PhysRevLett.115.246602 PACS numbers: 72.25.Dc, 72.25.Hg, 75.76.+j, 76.50.+g

Injecting and coherently controlling spin currents in nonmagnetic (NM) channels is a central goal of modern semiconductor spintronics [1–10]. Ferromagnetic resonance (FMR-)driven spin pumping [11–23] is an emerging method to dynamically inject pure spin current into a NM with no need for an accompanying charge current, promising substantial impacts on low energy cost or high efficiency electronics [1,2,11–13]. In contrast to conventional spin injection techniques that introduce a constant (dc) polarization component parallel to the magnetization of the ferromagnet (FM), FMR-driven spin pumping also injects a rotating (ac) component that is typically orders of magnitude larger than the dc component and oriented perpendicular to the equilibrium magnetization [11,23]. The presence of this large ac component renders the simple model of the FMR-pumped spin current as a traditional electrically driven dc spin current in the absence of charge incomplete. This situation is further complicated by the fact that while the bulk of experimental work on electrically driven spin injection relies on the measurement of a *spin accumulation* via the change in chemical potential at a magnetic detector [1–7], FMR-driven spin pumping studies have, to date, relied almost exclusively on measuring *spin currents* via a transverse voltage generated by the inverse spin-Hall effect (ISHE) [11–20]. As a result, there is to date no direct experimental comparison between these two regimes and no universal framework for understanding spin injection in both static (dc) and dynamic (ac) modalities.

Here we report measurements of both electrical spin injection and FMR-driven spin pumping in the same Si-based metal-oxide-semiconductor heterostructure through measurements of the spin accumulation voltage V_s. Comparison of V_s between these two spin injection mechanisms reveals an anomalously strong suppression of FMR-driven spin pumping with increasing out-of-plane field H^z_{app} that cannot be explained within existing models for dc spin injection. We propose that the large ac component of the spin current in the spin pumping approach is the source of this discrepancy, which arises from the interplay between this ac spin current and the inherent dynamics of the spin accumulation itself. These results lay the foundation for a universal model of spin injection and demonstrate the role of ac spin injection in determining the dynamics of the injected spin ensemble.

In our experiments, tunnel diodes are fabricated from Fe(10 nm)/MgO(1.3 nm)/Si(100) heterostructures grown by molecular beam epitaxy. The p-type Si substrates are semiconductor-on-insulator wafers with a 3 μm thick Si device layer containing 5×10^{18} cm^{-3} boron dopants, producing a room temperature resistivity of 2×10^{-2} Ωcm. The device is patterned by conventional photolithography techniques into a Fe/MgO/Si tunnel contact of 500 $\times$ 500 μm^2 lateral size, placed 1 mm away from Au reference contacts for voltage measurements. For both traditional three-terminal electrical spin injection and FMR-driven spin pumping measurements the samples are placed in the resonant cavity of a Bruker electron paramagnetic resonance spectrometer with resonant frequency $f = 9.85$ GHz and a dc magnetic field H_{app} applied along the x axis, as sketched in Fig. 1(a).

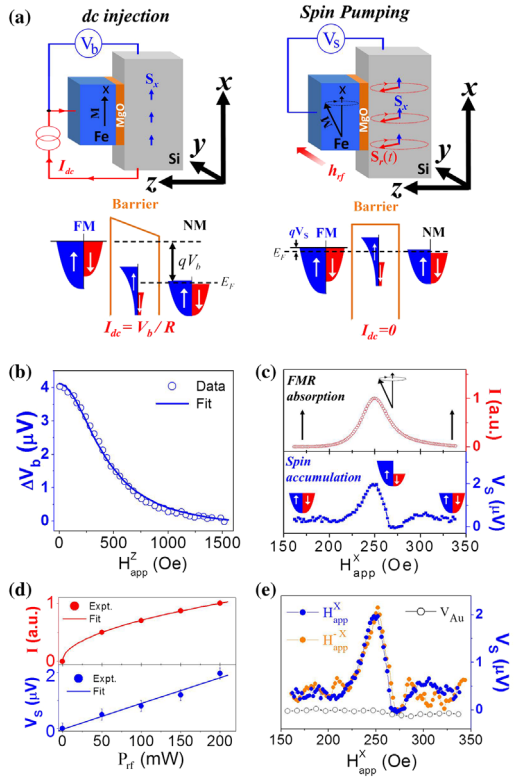

FIG. 1 (color online). (a) Schematic of experimental setup and band diagram of electrical injection (left-hand panel) and FMR-driven spin pumping (right-hand panel). (b) Hanle effect of dc (electrical) spin injection with 0.1 mA dc current applied. (c) FMR intensity (upper panel; arrows indicate state of the Fe magnetization) and spin-resolved voltage V_s (lower panel) as a function of applied magnetic field along the x axis. (d) FMR intensity (upper panel) and spin-resolved voltage (lower panel) as a function of rf power. (e) Solid symbols: V_s vs H_{app} when H_{app} is parallel or antiparallel with the x axis; open symbols indicate the voltage between two Au/Si reference contacts. All data are measured under the same experimental conditions.

For three-terminal measurements the current drive is turned on and the microwave field is turned off, while for FMR-driven spin pumping the current drive is turned off and the microwave field is turned on. This arrangement allows for the measurement of electrical and FMR-driven spin injection in the same device with identical contact geometry, interface electronic structure, and dc magnetic field geometry. In both cases, the resulting spin current induces an imbalance in the spin-resolved electrochemical potential and consequent spin accumulation given by $\Delta\mu_S = \mu_\uparrow - \mu_\downarrow$, where $\mu_\uparrow$ and $\mu_\downarrow$ are the chemical potentials of up and down spins, respectively. Using standard electrical spin detection techniques [4–6,24–29] the spin accumulation can be detected electrically by measuring the spin-resolved voltage V_s between Fe and Si:

$$V_S = \frac{P}{2e}\Delta\mu_S, \tag{1}$$

where P is the spin polarization of Fe and $\Delta\mu_S$ is assumed to be proportional to the component of the net spin polarization parallel to the magnetization, $\boldsymbol{M}$. Figure 1(b) shows the results of a traditional three-terminal Hanle measurement, with the expected suppression of spin polarization with increasing field [4–6,24–29]. Consistent with previous reports from our group and others [24–29], we extract an effective spin lifetime of 110 ps, and systematic studies reveal both the so-called inverted Hanle effect and current-voltage characteristics consistent with the presence of interface states mediating the spin transport between the Fe/MgO electrode and the Si channel (see Supplemental Material [30]). This suggests that the spin accumulation signal is dominated by the interface, rather than the bulk Si channel, which is consistent with previous reports [27–29]. Figure 1(c) shows both the inductively detected FMR signal from the Fe electrode (upper panel) and the response of V_s over the same field range (lower panel) in the presence of microwave excitation of 200 mW (the power used for all subsequent spin pumping measurements) and with no dc applied current and the sample placed in the center of a rectangular cavity (TE 102 mode). The spin accumulation voltage shows a clear response coincident with Fe FMR signal (with both symmetric and antisymmetric Lorentzian components) and an amplitude of roughly 2 μV. However, as has been established in earlier work involving ISHE detection of spin pumping [12–22], the presence of the microwave field has the potential to introduce a number of magnetoresistive and spin-thermal artifacts. We therefore turn our attention to a series of control measurements to further elucidate the origin of this signal.

Figure 1(d) shows the rf power P_{rf} dependence of the FMR intensity (upper panel) and V_s (lower panel) on resonance; the former is proportional to the square root of P_{rf} and the latter is linear with P_{rf} over the range 0–200 mW, consistent with ISHE detected spin pumping [18–20]. Further, as shown in Fig. 1(e), V_s is constant when $\boldsymbol{M}$ reverses, consistent with our local detection geometry wherein the injected spin is always parallel to the magnetization of the FM electrode and inconsistent with the response expected from ISHE generated voltages [18–20]. Measurement between two Au reference contacts [Fig. 1(e), open circles] further confirms that the signal is not from spurious microwave-induced voltages. A comprehensive analysis of other previously observed magnetotransport artifacts (see Supplemental Material [30]) yields similar results; i.e., the characteristics of these artifacts either qualitatively disagree with the symmetry of our observed signal or are quantitatively negligible for our specific measurement.

While the results of these control measurements are a strong indication that the response in V_s does in fact arise from FMR-driven spin pumping, the widely accepted gold standard for demonstrating the presence of a nonequilibrium spin accumulation is the presence of ensemble

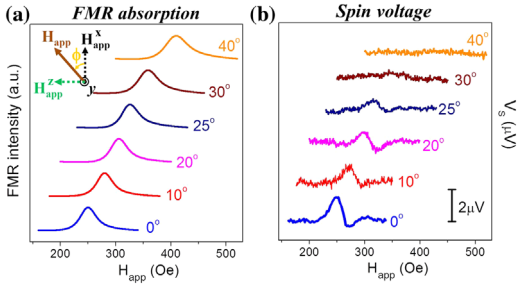

FIG. 2 (color online). (a) FMR intensity spectra at various magnetic field orientations Φ as described in the text. (b) V_s vs H_{app} measured at the same set of magnetic field orientations. The shift in FMR center frequency tracks the expected magnetization anisotropy of the Fe thin film; see text.

dephasing induced by a transverse dc magnetic field (the Hanle effect [1,4–6]). In the traditional Hanle geometry used to obtain the data shown in Fig. 1(b), the in-plane dc field (H^x_{app}) is set to zero while the out-of-plane component (H^z_{app}) is systematically varied. However, measurements of FMR-driven spin pumping present an additional constraint: while increasing the out-of-plane component of the dc magnetic field (H^z_{app}) the in-plane component (H^x_{app}) must be finite and tuned the resonant field for FMR in the electrode. The resulting vector magnetic field varies in both magnitude and angle with respect to the sample plane, resulting in a slightly modified version known as the oblique Hanle geometry [24,28] [Fig. 2(a), inset].

Because of the strong demagnetization field of our thin-film geometry (∼2.2 T), the orientation of the magnetization lags the orientation of the applied field, remaining almost entirely in plane (the maximum estimated deviation is 2°). Since the injected spins (both ac and dc terms) should follow the corresponding component of $\boldsymbol{M}$, the relative angle between the spin ensemble and the magnetization should not change with the tilt of $\boldsymbol{M}$, leading to a constant intensity of the FMR response. Figure 2(a) shows the FMR spectrum for different angles Φ; the resonant field H_{FMR} changes from 250 to 400 G as Φ changes from 0 to 40 deg. This increase is consistent with the fact that the in-plane component of H primarily determines the resonance condition; so as Φ increases, a larger total applied field is therefore required to achieve resonance (see Supplemental Material [30]). Figure 2(b) shows V_s vs H_{app} over the same angular range. The peak position of V_s shifts in parallel with the FMR spectrum, but the peak value decreases with increasing H_z and vanishes at an angle of approximately 40 deg. Note that this suppression of V_s further rules out both magnetoresistive and spin-thermal artifacts as both the microwave environment and the FMR in the Fe electrode are effectively unchanged by this rotation of the magnetic field. We repeat this oblique Hanle measurement for the electrical injection geometry, with the total applied field at a given angle selected for consistency with the shifting of the FMR resonance. The full data set can be found in the

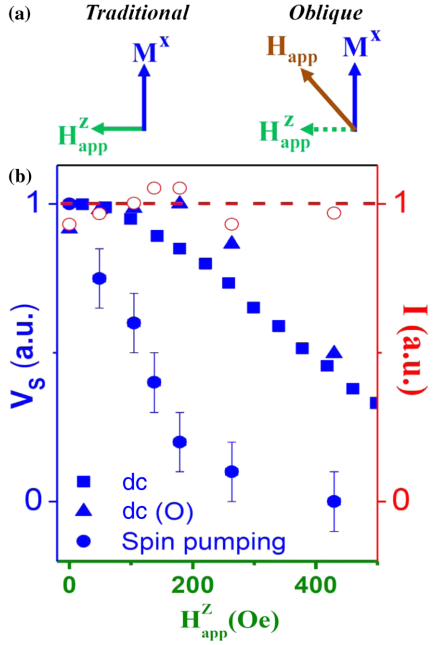

FIG. 3 (color online). (a) Schematics of traditional and oblique Hanle geometries. (b) V_s vs H^z_{app} for electrical injection (filled squares and triangles) and spin pumping (filled circles), filled triangles represent electrical injection measured in an oblique geometry that is the same as for spin pumping, open circles are FMR absorption as a function of H^z_{app} (with ∼10% variation for different Φ), the dashed line is a guide to the eye.

Supplemental Material [30] and a summary of the results is presented in Fig. 3, with the general result that there is not a significant difference between the traditional and oblique Hanle response for the electrical injection geometry in these devices.

It is tempting to ascribe the suppression of the FMR-driven spin pumping signal entirely to Hanle-type dephasing of the injected spin ensemble. However, we note that in this oblique geometry the spin ensemble will relax along the vector magnetic field, resulting in a dc component of the spin accumulation with a finite projection along the magnetization of the detector $\boldsymbol{M}$. As a result, even for an infinite spin lifetime, Hanle dephasing in the oblique geometry can never lead to a complete suppression of the spin polarization. This discrepancy is even more evident if one plots the magnitude of the V_s generated by spin pumping (Fig. 3, filled circles) on the same field scale as V_s for electrical injection (Fig. 3, filled squares). For ease of comparison with the electrical injection measurements, we plot only the z component of the full dc field for the spin pumping measurements. Plotting the same data vs the total applied field yields the same qualitative trends (see Supplemental Material [30]). Measuring the electrically injected V_s under the same oblique field conditions as used for the FMR measurement (Fig. 3, filled triangles; see Supplemental Material [30]) demonstrates that this discrepancy is not due to the oblique geometry. These results

clearly show that there is a fundamental difference between electrical and FMR-driven spin injection, and that our existing models for the dynamic evolution of FMR injected spin ensembles is incomplete.

We attempt to understand this discrepancy by building on the formalism developed for electrical injection in the three-terminal geometry [4]. Specifically, in electrical injection the spin current is taken to be constant in both magnitude and orientation while FMR-driven spin pumping has both an ac and a dc source term, corresponding to the deviation of the precessional cone of the magnetization $\boldsymbol{M}$ from its static projection. For the microwave field strength used in this experiment, this precession results in a maximum cone angle of 1°, as determined from the relation $\theta = (2h_{\mathrm{rf}}/\sqrt{3}\Delta H)$, where $h_{\mathrm{rf}} = 0.3$ Oe for our spectrometer and ΔH for our Fe sample is 30 Oe. From this, simple trigonometry predicts a ratio of roughly 100:1 between the ac and dc components of the injected spin. These two components yield a time-dependent spin current $\mathbf{J_s}$ (t) [11,23]:

$$\mathbf{J}_s(t) = \mathbf{J}_x + \mathbf{J}_{r(y,z)}(t) = J_x\hat{\mathbf{x}} + J_r(\hat{\mathbf{y}}\cos\omega t + \hat{\mathbf{z}}\sin\omega t), \tag{2}$$

where J_x and J_r are the magnitudes of dc and ac spin current, respectively, and ω is the angular velocity of FMR. Keeping in mind the invariance of the FMR intensity as a function of the angle of the applied field shown in Fig. 3, we take this source term to also be independent of applied field angle; we find the time-dependent spin polarization at the interface to be

$$\begin{aligned}\mathbf{S} &= \mathbf{S}_x + \mathbf{S}_r(t) \\ &= \hat{\mathbf{x}}J_x\tau + \frac{J_r\tau}{[1+(\omega\tau)^2]^{1/2}}[\hat{\mathbf{y}}\cos(\omega t\text{-}\beta) + \hat{\mathbf{z}}\sin(\omega t\text{-}\beta)],\end{aligned} \tag{3}$$

where τ is the spin lifetime and the phase lag between the FMR precession and the precession of the injected spins is given by $\beta = \arctan(\omega\tau)$. In the presence of a magnetic field applied in the xz plane, the spin ensemble along the x axis (the measurement direction in this experiment) is given by

$$\begin{aligned}S_x^{\mathrm{SP}}(t) = &\frac{J_x\tau[1+(\omega_x\tau)^2]}{1+(\omega_x\tau)^2+(\omega_z\tau)^2} \\ &+ \frac{J_r\tau[\cos\omega t + (\omega_x-\omega)\tau\sin\omega t]\omega_z\tau}{1+[(\omega_x-\omega)\tau]^2+(\omega_z\tau)^2},\end{aligned} \tag{4}$$

where ω_x and ω_z represent the x and z components of the magnetic field and the first and second terms represent the dc and ac components of the spin ensemble, respectively.

A qualitative depiction of the behavior of this spin ensemble is shown in Fig. 4(a). In contrast to previous studies, in the measurements presented here both the magnetization of the injector and the spin polarization of the injected ensemble have dc and ac components. In principle, this provides an additional channel for the generation of a spin accumulation voltage due to the possible alignment of the precessing Fe magnetization with the precessing spin ensemble. However, in practice this contribution to V_s is negligible in our measurements (see Supplemental Material [30]).

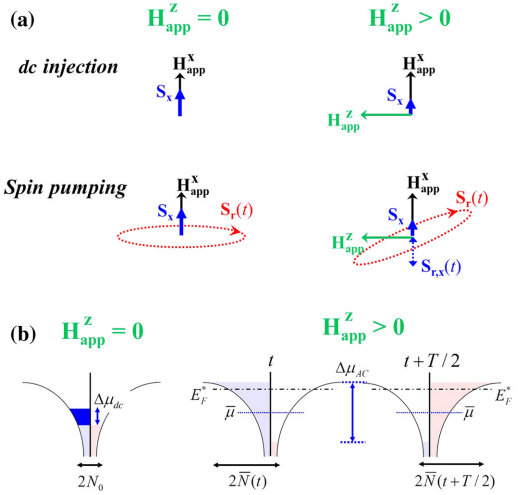

FIG. 4 (color online). (a) Schematics of the effect of an oblique magnetic field for electrical and FMR-driven spin injection. Solid blue arrows represents the dc component of spins along the x axis and the dashed arrows represent the ac component of spins. (b) Band diagram of spin accumulation when $H^z_{\mathrm{app}} = 0$ or $H^z_{\mathrm{app}} > 0$ at certain time t and at half period later.

As a result, when the dc applied magnetic field is maintained parallel to the magnetization, and the large ac component of the injected spin ensemble is everywhere perpendicular to the dc component of the magnetization of the detector, it does not contribute directly to the measured spin accumulation voltage. However, when the dc applied magnetic field is applied at some angle Φ [see Fig. 2(a)], the z component of the field will lead to a canting of the ac component such that it has an oscillating projection along the measurement axis (i.e., along the direction of the dc magnetization). While the development of an analytic formalism for the time dependence of the spin ensemble is relatively straightforward, it is significantly more challenging to obtain an analytic expression for the resulting change in chemical potential $\Delta\mu$ arising from this dynamic spin population. In particular, the experimental observable V_s can be related to $\Delta\mu$ using Eq. (1), but $\Delta\mu$ itself is proportional to S_x^{SP} through the density of states of the channel. While a full analytic description of this dynamic density of states is beyond the scope of this work, there are several qualitative observations that lay the foundation for a conceptual framework for understanding this phenomenon.

For example, a consequence of this dynamic chemical potential can be found in considering previous work on electrical spin injection in similar structures [27] that

clearly indicates that the relevant density of states is both relatively narrow (as compared to bulk Si) and strongly varying near the Fermi energy. The implications of this strong variation are shown schematically in Fig. 4(b). First, the strong variation near the Fermi energy implies that flipping a single spin from the minority to the majority spin bands will move the minority band *down* more than it will move the majority band *up*, due to the larger number of available states as energy increases. This results in a net downward shift of the average chemical potential relative to the equilibrium Fermi energy, in direct opposition to the $\Delta\mu$ expected from spin injection. This shift has been observed in the measurement of a spin polarization using a nonmagnetic electrode [36], and will result in a net negative offset to the expected Hanle dephasing signal in our measurements. This field-dependent suppression of V_s will appear to narrow the Hanle signal. Note that this mechanism is similar in origin to the dependence on dn/dE of the Seebeck effect in thermal transport studies [36,37].

In summary, we report a direct comparison of the spin accumulation voltage V_s in the presence of both electrical and FMR-driven spin injection in a single device. We observe an anomalously strong suppression of V_s as a function of the out-of-plane component of the applied magnetic field H^z_{app} that points to fundamental differences in the spin injection or detection processes in these two geometries. In particular, we propose that the presence of an ac component in the FMR-driven spin current, which is predicted to be $100\times$ stronger than the dc component, requires a more nuanced view of the interplay between the dynamics of the injector and the interface. This interplay, wherein the dynamics of both the injector and the interface play a significant role in the spin accumulation, represents a new regime for spin injection that is not well described by existing models of either FMR-driven spin pumping or electrical spin injection.

This material is based upon work supported by the Center for Emergent Materials, a NSF MRSEC under Award No. DMR-1420451 (Y. P., P. M. O., J. B., A. G. S., R. K. K., M. E. F., P. C. H., and J. P.), and by the Department of Energy through Grants No. DE-FG02-03ER46054 (R. A.) and No. DE-SC0001304 (E. J.-H.). Technical support is provided by the NanoSystems Laboratory at The Ohio State University. The authors thank Andrew Berger and Steven Tjung for discussions and assistance.

*puyong@gmail.com
†ejh@mps.ohio-state.edu

[1] I. Žutić, J. Fabian, and S. Das Sarma, Rev. Mod. Phys. **76**, 323 (2004).
[2] D. D. Awschalom and M. E. Flatté, Nat. Phys. **3**, 153 (2007).
[3] I. Appelbaum, B. Huang, and D. J. Monsma, Nature (London) **447**, 295 (2007).
[4] S. P. Dash, S. Sharma, R. S. Patel, M. P. de Jong, and R. Jansen, Nature (London) **462**, 491 (2009).
[5] F. J. Jedema, H. B. Heersche, A. T. Filip, J. Baselmans, and B. J. van Wees, Nature (London) **416**, 713 (2002).
[6] X. Lou, C. Adelmann, S. A. Crooker, E. S. Garlid, J. Zhang, K. S. Madhukar Reddy, S. D. Flexner, C. J. Palmstrøm, and P. A. Crowell, Nat. Phys. **3**, 197 (2007).
[7] B. T. Jonker, G. Kioscoglou, A. T. Hanbicki, C. H. Li, and P. E. Thompson, Nat. Phys. **3**, 542 (2007).
[8] Y. K. Kato, R. C. Myers, A. C. Gossard, and D. D. Awschalom, Science **306**, 1910 (2004).
[9] S. O. Valenzuela and M. Tinkham, Nature (London) **442**, 176 (2006).
[10] L. Liu, C.-F. Pai, Y. Li, H. W. Tseng, D. C. Ralph, and R. A. Buhrman, Science **336**, 555 (2012).
[11] Y. Tserkovnyak, A. Brataas, and G. E. W. Bauer, Phys. Rev. Lett. **88**, 117601 (2002).
[12] E. Saitoh, M. Ueda, H. Miyajima, and G. Tatara, Appl. Phys. Lett. **88**, 182509 (2006).
[13] Y. Tserkovnyak, A. Brataas, G. Bauer, and B. I. Halperin, Rev. Mod. Phys. **77**, 1375 (2005).
[14] Y. Kajiwara *et al.*, Nature (London) **464**, 262 (2010).
[15] H. Kurebayashi, O. Dzyapko, V. E. Demidov, D. Fang, A. J. Ferguson, and S. O. Demokritov, Nat. Mater. **10**, 660 (2011).
[16] C. W. Sandweg, Y. Kajiwara, A. V. Chumak, A. A. Serga, V. I. Vasyuchka, M. B. Jungfleisch, E. Saitoh, and B. Hillebrands, Phys. Rev. Lett. **106**, 216601 (2011).
[17] F. D. Czeschka *et al.*, Phys. Rev. Lett. **107**, 046601 (2011).
[18] K. Ando *et al.*, J. Appl. Phys. **109**, 103913 (2011); K. Ando, S. Takahashi, J. Ieda, H. Kurebayashi, T. Trypiniotis, C. H. W. Barnes, S. Maekawa, and E. Saitoh, Nat. Mater. **10**, 655 (2011); K. Ando and E. Saitoh, Nat. Commun. **3**, 629 (2012).
[19] E. Shikoh, K. Ando, K. Kubo, E. Saitoh, T. Shinjo, and M. Shiraishi, Phys. Rev. Lett. **110**, 127201 (2013).
[20] S. Dushenko, M. Koike, Y. Ando, T. Shinjo, M. Myronov, and M. Shiraishi, Phys. Rev. Lett. **114**, 196602 (2015).
[21] M. V. Costache, M. Sladkov, S. M. Watts, C. H. van der Wal, and B. J. van Wees, Phys. Rev. Lett. **97**, 216603 (2006).
[22] B. Heinrich, C. Burrowes, E. Montoya, B. Kardasz, E. Girt, Y.-Y. Song, Y. Sun, and M. Wu, Phys. Rev. Lett. **107**, 066604 (2011).
[23] H. J. Jiao and G. E. W. Bauer, Phys. Rev. Lett. **110**, 217602 (2013).
[24] S. P. Dash, S. Sharma, J. C. Le Breton, J. Peiro, H. Jaffrès, J.-M. George, A. Lemaître, and R. Jansen, Phys. Rev. B **84**, 054410 (2011).
[25] C. H. Li, O. van't Erve, and B. T. Jonker, Nat. Commun. **2**, 245 (2011).
[26] N. W. Gray and A. Tiwaria, Appl. Phys. Lett. **98**, 102112 (2011).
[27] Y. Pu, J. Beardsley, P. M. Odenthal, A. G. Swartz, R. K. Kawakami, P. C. Hammel, E. Johnston-Halperin, J. Sinova, and J. P. Pelz, Appl. Phys. Lett. **103**, 012402 (2013).
[28] K. Jeon, Y.-H. Park, S.-Y. Park, and S.-C. Shin, Phys. Rev. B **87**, 195311 (2013).
[29] M. Tran, H. Jaffrès, C. Deranlot, J.-M. George, A. Fert, A. Miard, and A. Lemaître, Phys. Rev. Lett. **102**, 036601 (2009).

[30] See Supplemental Material at http://link.aps.org/supplemental/10.1103/PhysRevLett.115.246602, which includes Refs. [31–35], for further discussion of control experiments and modeling.

[31] T. Uemura, K. Kondo, J. Fujisawa, K.-i. Matsuda, and M. Yamamoto, Appl. Phys. Lett. **101**, 132411 (2012); O. Txoperena, M. Gobbi, A. Bedoya-Pinto, F. Golmar, X. Sun, L. E. Hueso, and F. Casanova, Appl. Phys. Lett. **102**, 192406 (2013); H. N. Tinkey, P. Li, and I. Appelbaum, Appl. Phys. Lett. **104**, 232410 (2014).

[32] Y. Song and H. Dery, Phys. Rev. Lett. **113**, 047205 (2014); Z. Yue, M. C. Prestgard, A. Tiwari, and M. E. Raikh, Phys. Rev. B **91**, 195316 (2015).

[33] O. Txoperena, Y. Song, L. Qing, M. Gobbi, L. E. Hueso, H. Dery, and F. Casanova, Phys. Rev. Lett. **113**, 146601 (2014); A. Swartz, S. Harashima, Y. Xie, D. Lu, B. Kim, C. Bell, Y. Hikita, and H. Y. Hwang, Appl. Phys. Lett. **105**, 032406 (2014).

[34] H. Wang, C. Du, P. Chris Hammel, and F. Yang, Appl. Phys. Lett. **104**, 202405 (2014).

[35] K. Olejnik, J. Wunderlich, A. C. Irvine, R. P. Campion, V. P. Amin, J. Sinova, and T. Jungwirth, Phys. Rev. Lett. **109**, 076601 (2012).

[36] C. Geppert *et al.*, arXiv:1402.2638; I. J. Vera-Marun, V. Ranjan, and B. J. van Wees, Nat. Phys. **8**, 313 (2012).

[37] N. F. Mott and H. Jones, *The Theory of the Properties of Metals and Alloys* (Dover Publications, New York, 1958); M. Jonson and G. D. Mahan, Phys. Rev. B **21**, 4223 (1980).